

Pyrin inflammasome activation and RhoA signaling in the autoinflammatory diseases FMF and HIDS

Yong Hwan Park, Geryl Wood, Daniel L Kastner & Jae Jin Chae

Mutations in the genes encoding pyrin and mevalonate kinase (MVK) cause distinct interleukin-1 β (IL-1 β)-mediated autoinflammatory diseases: familial Mediterranean fever (FMF) and hyperimmunoglobulinemia D syndrome (HIDS). Pyrin forms an inflammasome when mutant or in response to bacterial modification of the GTPase RhoA. We found that RhoA activated the serine-threonine kinases PKN1 and PKN2 that bind and phosphorylate pyrin. Phosphorylated pyrin bound to 14-3-3 proteins, regulatory proteins that in turn blocked the pyrin inflammasome. The binding of 14-3-3 and PKN proteins to FMF-associated mutant pyrin was substantially decreased, and the constitutive IL-1 β release from peripheral blood mononuclear cells of patients with FMF or HIDS was attenuated by activation of PKN1 and PKN2. Defects in prenylation, seen in HIDS, led to RhoA inactivation and consequent pyrin inflammasome activation. These data suggest a previously unsuspected fundamental molecular connection between two seemingly distinct autoinflammatory disorders.

Mutations in the genes encoding proteins constituting inflammasomes or regulating inflammasome activation cause IL-1 β -mediated autoinflammatory diseases^{1,2}. FMF and HIDS are two such disorders caused by missense mutations of *MEFV* and *MVK*, which encode pyrin and mevalonate kinase (MVK), respectively^{3,4}. Pyrin spontaneously forms an inflammasome, dependent on the adaptor ASC, when mutant⁵ or in response to bacterial toxins⁶, and MVK is a key enzyme in the mevalonate pathway, producing isoprenoids⁷ such as geranylgeranyl pyrophosphate. However, the exact molecular mechanism of pyrin inflammasome activation, as well as the molecular pathology of FMF and HIDS, is unknown.

Published genetic studies of FMF in Sephardi Jewish families with severe disease revealed a recessive mode of inheritance^{3,8,9}, suggesting that FMF might be caused by loss-of-function mutations in pyrin. However, the availability of genetic testing has led to both the definition of a biochemical phenotype in asymptomatic heterozygotes¹⁰ and the recognition that as many as 30% of patients with clinical FMF have only a single demonstrable mutation in *MEFV*^{11–13}. Indeed, several cases of apparently dominantly inherited FMF have been reported^{14,15}, whereas null mutations are extremely rare. Moreover, pyrin-deficient mice develop normally and exhibit no overt phenotype⁵, arguing against a loss-of-function model for FMF. Data from knock-in mice harboring FMF-associated mutations of the gene encoding human pyrin strongly support a gain-of-function model with a gene-dosage effect, with the mutant pyrin inducing an ASC-dependent inflammasome and IL-1 β -mediated systemic inflammation⁵.

Certain bacterial toxins that inactivate Rho GTPases induce IL-1 β production by the pyrin inflammasome through an indirect mechanism that does not involve an interaction between pyrin and Rho GTPases⁶. Our results elucidate a pathway by which RhoA activation induces

downstream kinases, pyrin phosphorylation and the resulting inhibitory binding of phosphorylated pyrin by 14-3-3 proteins, and demonstrate the effects of pyrin and MVK mutations in relieving the tonic inhibition of the pyrin inflammasome. Bacterial sensing by pyrin therefore represents an example in which innate immunity in mammals is triggered by an indirect process that is similar to the 'guard' mechanism in plants^{16,17}.

RESULTS

RhoA activity suppresses pyrin inflammasome activation

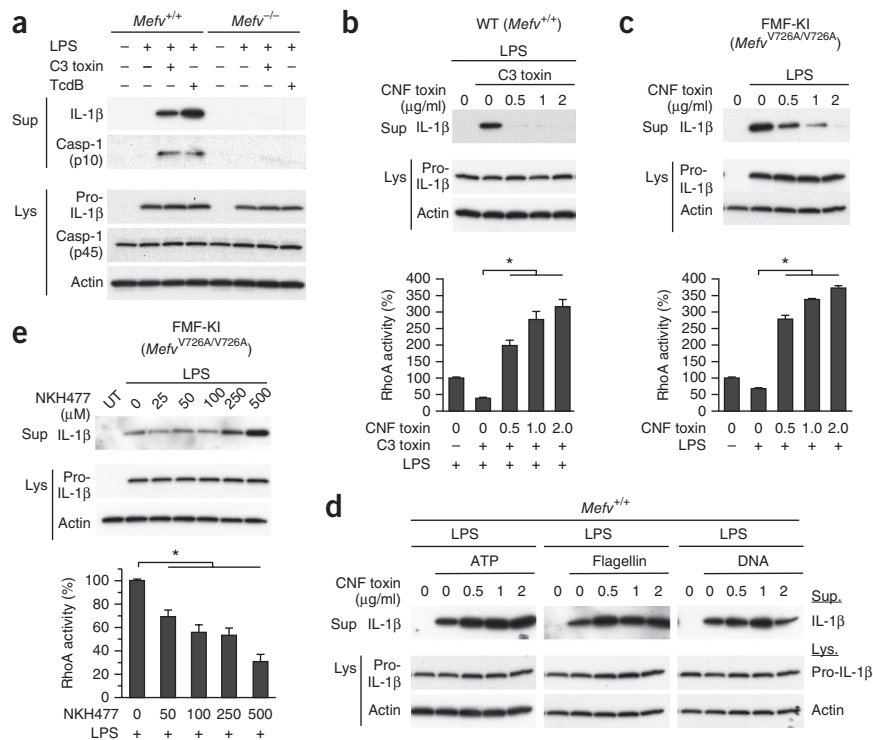
Bacterial toxins that modify RhoA induce inflammasome formation by wild-type pyrin⁶. These bacterial toxins mediate the glycosylation, adenylation, ADP-ribosylation or deamidation of various residues in the switch I region of RhoA, inhibiting guanine nucleotide binding and GTPase activity. Taken together with the absence of evidence for direct interaction between pyrin and modified RhoA⁶, the data suggest that the pyrin inflammasome is activated by the inhibition of downstream RhoA signaling pathways. Thus, we initially explored the correlation between RhoA activity and the pyrin inflammasome by studying bone-marrow-derived macrophages (BMDMs) in which pyrin had been induced by lipopolysaccharide (LPS)¹⁸.

Consistent with published findings⁶, the clostridial TcdB and C3 toxins induced caspase-1 activation and bioactive IL-1 β release from LPS-primed BMDMs by a pathway that was dependent on pyrin, ASC and caspase-1 but independent of NLRP3, NLRC4 and AIM2 (Fig. 1a and Supplementary Fig. 1a). In contrast, C3-toxin-induced IL-1 β release was substantially diminished when the BMDMs were treated with calpeptin, an indirect upstream RhoA activator¹⁹, or bacterial cytotoxic necrotizing factor (CNF) toxin, a direct RhoA activator that deamidates glutamine-63 of Rho^{20,21} (Fig. 1b and Supplementary Fig. 1b–d).

Inflammatory Disease Section, Metabolic, Cardiovascular and Inflammatory Disease Genomics Branch, National Human Genome Research Institute, US National Institutes of Health, Bethesda, Maryland, USA. Correspondence should be addressed to D.L.K. (kastnerd@mail.nih.gov) or J.J.C. (chaej@mail.nih.gov).

Received 11 February; accepted 31 March; published online 6 June 2016; doi:10.1038/ni.3457

Figure 1 The pyrin inflammasome is activated by inactivation of RhoA. **(a)** Immunoblot analysis of culture supernatants (sup) and lysates (Lys) of wild-type (WT) or *Mefv*^{-/-} BMDMs primed for 6 h with LPS (1 μg/ml) and either C3 toxin (0.5 μg/ml) or TcdB (0.5 μg/ml). **(b,c)** IL-1β release (top) and activated RhoA (bottom) in wild-type BMDMs treated with LPS, C3 toxin and CNF toxin **(b)** and *Mefv*^{V726A/V726A} BMDMs treated for 6 h with LPS plus CNF toxin **(c)**; RhoA activity is presented relative to that in LPS-treated cells **(b)** or untreated cells **(c)**. **(d)** IL-1β release from wild-type BMDMs treated for 5 h with LPS plus various concentrations of CNF toxin (above lanes) and administered ATP (2 mM) for 0.5 h, flagellin (0.5 μg/ml with 25 μl/ml DOTAP) for 1 h or double-stranded DNA (dsDNA, 1 μg/ml with 2.5 μl/ml Lipofectamine 2000) for 1 h. **(e)** IL-1β release (top) and activated RhoA (bottom) in LPS-primed *Mefv*^{V726A/V726A} BMDMs left untreated (UT) treated for 1 h with various doses (above lanes and horizontal axis) of NKH477 (RhoA activity presented as in **b**). **P* ≤ 0.005 (unpaired two-tailed *t* test). Data are representative of at least three independent experiments (**a,d**, and **b,c,e**, top) or one experiment with six mice (**b,c**) or eight mice (**e**) (**b,c,e**, bottom; mean + s.e.m.).



RhoA activators also reduced IL-1β release from the LPS-primed BMDMs of FMF knock-in mice harboring the *MEFV* mutation encoding the V726A substitution (*Mefv*^{V726A/V726A}), in which the pyrin inflammasome is constitutively activated⁵ (**Fig. 1c** and **Supplementary Fig. 1e**). On the other hand, the activation of RhoA had no suppressive effect on the NLRC4 or AIM2 inflammasomes (**Fig. 1d** and **Supplementary Fig. 1f**). The NLRC3 inflammasome was

also not inhibited by the CNF toxin, despite its inhibition by calpeptin (**Fig. 1d** and **Supplementary Fig. 1f**).

Another line of evidence supporting the inverse relationship between RhoA activation and pyrin inflammasome induction follows from a published study of the inhibition of the NLRP3 inflammasome by intracellular cyclic AMP (cAMP), in which cAMP was found to accentuate IL-1β production by peripheral blood mononuclear cells (PBMCs) from patients with FMF²². cAMP is known to induce phosphorylation

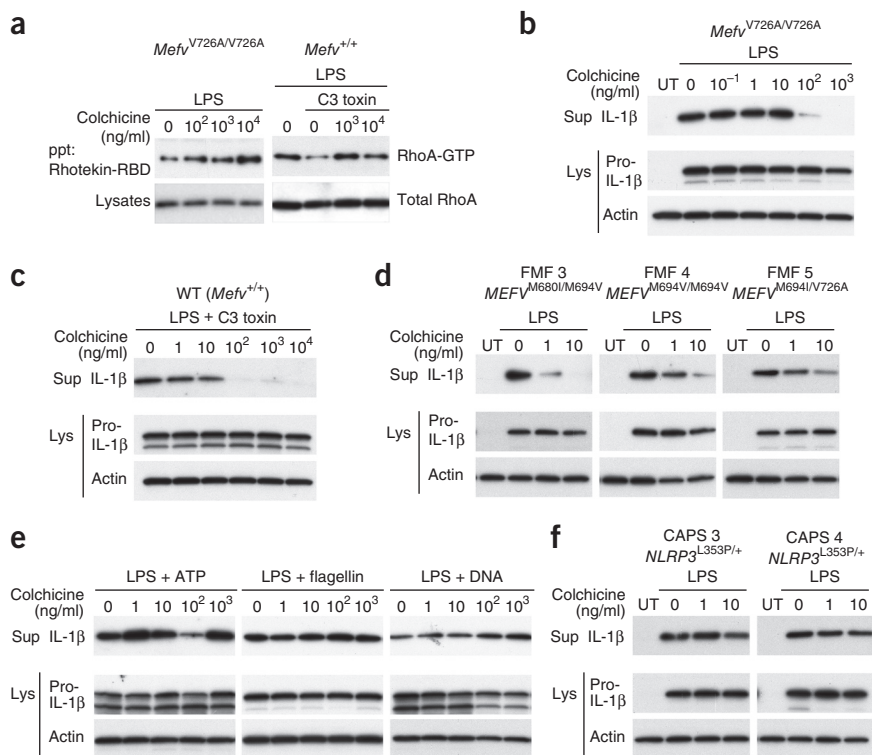
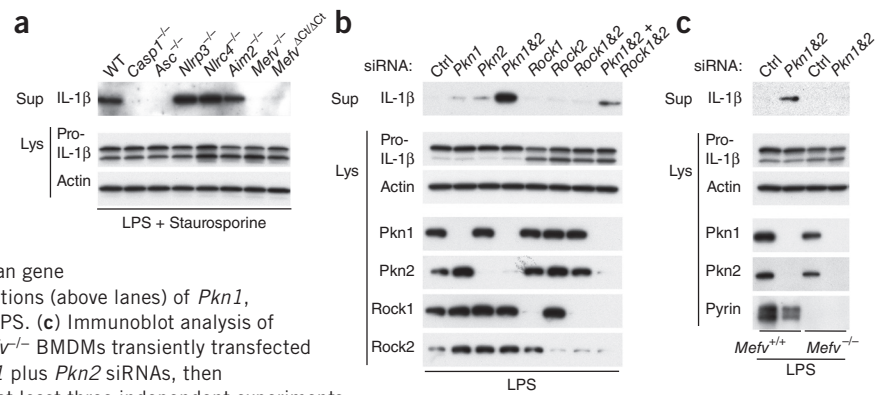


Figure 2 Colchicine suppresses the pyrin inflammasome. **(a)** Precipitation assay of activated RhoA (GTP-RhoA) in *Mefv*^{V726A/V726A} or wild-type (*Mefv*^{+/+}) BMDMs treated with various concentrations of colchicine (above lanes) with or without C3 toxin. **(b)** Immunoblot analysis of culture supernatants and lysates of LPS-primed *Mefv*^{V726A/V726A} BMDMs treated with various concentrations (above lanes) of colchicine. **(c)** Immunoblot analysis of culture supernatants and lysates of wild-type BMDMs treated with LPS, C3 toxin and various concentrations (above lanes) of colchicine. **(d,f)** Immunoblot analysis of culture supernatants and lysates of PBMCs obtained from patients with FMF (3, 4 and 5; **d**) or CAPS (3 and 4; **f**) with various mutations (above blots) in *MEFV* (**d**) or *NLRP3* (**f**) and treated for 6 h with LPS plus various doses (above lanes) of colchicine. **(e)** Immunoblot analysis of culture supernatants and lysates of wild-type BMDMs primed for 3 h with LPS and then treated with various concentrations (above lanes) of colchicine and ATP (2 mM) for 0.5 h, flagellin (0.5 μg/ml with 25 μl/ml DOTAP) for 1 h or dsDNA (1 μg/ml with 2.5 μl/ml of Lipofectamine 2000) for 1 h. Data are representative of at least three independent experiments (**a-c,e**) or one experiment (**d,f**).

Figure 3 Inhibition of RhoA effector kinases activates the pyrin inflammasome.

(a) Immunoblot analysis of culture supernatants and lysates of LPS-primed wild-type, *Casp1*-, *Asc*-, *Nlrp3*-, *Nlrc4*-, *Aim2*- or *Mefv*-deficient, or *Mefv*^{ACUΔCt} (C-terminal pyrin truncation) BMDMs treated for 1 h with staurosporine (1 μM). (b) Immunoblot analysis of culture supernatants and lysates of BMDMs transiently transfected with negative control siRNA with

no substantial sequence similarity to mouse or human gene sequences (Ctrl) or siRNA targeting various combinations (above lanes) of *Pkn1*, *Pkn2*, *Rock1* and *Rock2*, then treated for 8 h with LPS. (c) Immunoblot analysis of culture supernatants and lysates of wild-type or *Mefv*^{-/-} BMDMs transiently transfected with negative control siRNA or siRNA targeting *Pkn1* plus *Pkn2* siRNAs, then treated for 8 h with LPS. Data are representative of at least three independent experiments.



of RhoA at Ser188 through protein kinase A (PKA), resulting in the translocation of membrane-associated RhoA toward the cytosol^{23,24}. The increase of cAMP synthesis by the adenylate cyclase (ADCY) activator NKH477 (a water-soluble analog of forskolin) potentiated IL-1β release from PBMCs of patients with FMF (Supplementary Fig. 2a), whereas it moderately inhibited IL-1β release from PBMCs of patients with cryopyrin-associated periodic syndrome (CAPS) or ATP-treated wild-type mouse BMDMs (Supplementary Fig. 2b,c). Indeed, we observed a dose-dependent decrease in RhoA-GTP activity and an increase in IL-1β release from the LPS-primed BMDMs of *Mefv*^{V726A/V726A} mice in response to ADCY activation (Fig. 1e). In conclusion, the data from both human and mouse leukocytes that were subjected to bacterial toxins and pharmacologic agents support the proposal of an inverse relationship between RhoA activity and pyrin inflammasome activation.

Colchicine suppresses the pyrin inflammasome

We next examined the effect of colchicine on the pyrin inflammasome, as colchicine is a known activator for RhoA and an effective prophylaxis for FMF inflammatory attacks. In the cytosol, colchicine binds to tubulin and depolymerizes microtubules, resulting in the release of the RhoA activator guanine-nucleotide-exchange factor (GEF)-H1, which is inactive when bound to microtubules²⁵. Indeed, colchicine either activated RhoA or reversed the inhibition of RhoA activity by C3 toxin in LPS-primed BMDMs (Fig. 2a). Consistent with previous results showing an inverse relationship between RhoA activity and pyrin inflammasome activation, we observed that colchicine inhibited the constitutive IL-1β release from BMDMs of *Mefv*^{V726A/V726A} mice and C3 toxin-induced IL-1β release from

LPS-primed BMDMs (Fig. 2b,c). In addition, we also observed inhibition of IL-1β release by colchicine from PBMCs of patients with FMF (Fig. 2d). In contrast, colchicine had no consistent dose-dependent inhibitory effect on NLRP3, NLRC4 or AIM2 inflammasome activation (Fig. 2e) or the constitutive IL-1β release from the PBMCs of patients with CAPS (Fig. 2f), although it has been reported that colchicine inhibits NLRP3 inflammasome-induced IL-1β release at higher concentrations²⁶. These data suggest an explanation for the exquisite specificity of colchicine for FMF among the monogenic autoinflammatory diseases.

RhoA effector kinases suppress pyrin inflammasome activation

Given that the pyrin inflammasome is activated by inactivation of RhoA, we hypothesized that a signaling pathway downstream of RhoA may suppress the pyrin inflammasome. A number of proteins have been identified as being effectors of RhoA, most notably kinases such as ROCKs and PKNs that belong to the protein kinase C (PKC) superfamily. It is noteworthy that staurosporine, a potent inhibitor of PKC and an inducer of cell death, stimulates IL-1β release from LPS-primed macrophages through an unknown inflammasome activation²⁷. We found that staurosporine-induced IL-1β release was independent of the NLRP3, NLRC4 or AIM2 inflammasomes, but was dependent on the pyrin inflammasome (Fig. 3a and Supplementary Fig. 3a), suggesting that the pyrin inflammasome might be activated when a Rho effector kinase is inhibited.

To find RhoA effector kinases that regulate the pyrin inflammasome, we knocked down the genes encoding the Rho effector kinases PKNs and ROCKs in mouse BMDMs using small interfering RNA (siRNA). Knockdown of *Pkn1* or *Pkn2* in LPS-primed BMDMs

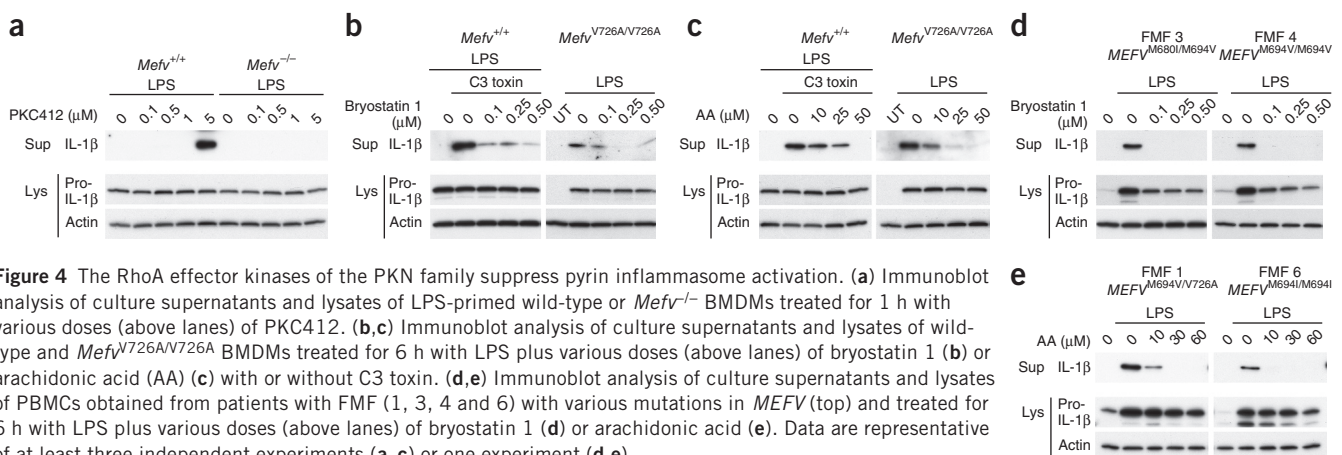
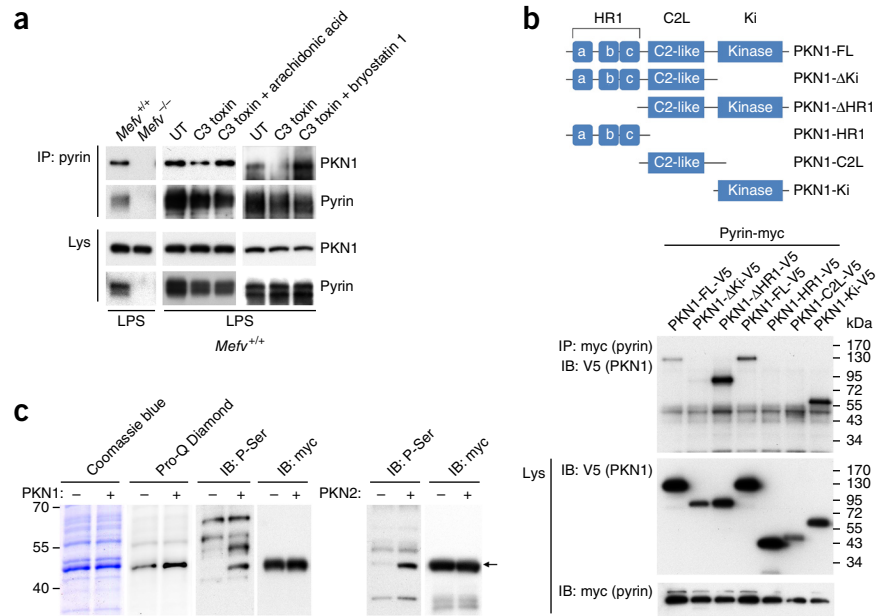


Figure 4 The RhoA effector kinases of the PKN family suppress pyrin inflammasome activation. (a) Immunoblot analysis of culture supernatants and lysates of LPS-primed wild-type or *Mefv*^{-/-} BMDMs treated for 1 h with various doses (above lanes) of PKC412. (b,c) Immunoblot analysis of culture supernatants and lysates of wild-type and *Mefv*^{V726A/V726A} BMDMs treated for 6 h with LPS plus various doses (above lanes) of bryostatin 1 (b) or arachidonic acid (AA) (c) with or without C3 toxin. (d,e) Immunoblot analysis of culture supernatants and lysates of PBMCs obtained from patients with FMF (1, 3, 4 and 6) with various mutations in *MEFV* (top) and treated for 6 h with LPS plus various doses (above lanes) of bryostatin 1 (d) or arachidonic acid (e). Data are representative of at least three independent experiments (a–c) or one experiment (d,e).

Figure 5 PKNs bind and phosphorylate pyrin.

(a) Immunoblot analysis of PKN1 and pyrin in lysates of LPS-primed wild-type and *Mefv*^{-/-} BMDMs or LPS-primed wild-type BMDMs treated with C3 toxin, C3 toxin and arachidonic acid, or C3 toxin and bryostatin 1, assessed after immunoprecipitation with antibody to pyrin. (b) Immunoblot analysis (with antibody to V5 (PKN1)) of lysates of 239T cells transiently expressing human pyrin and full-length PKN1 or various deletion mutants of PKN1 (above lanes), assessed after immunoprecipitation with antibody to Myc (pyrin) (top) and in lysates without immunoprecipitation (bottom). Above blots, full-length (FL) PKN1 and its deletion mutants. (c) Phosphorylation of Myc- and His-tagged N-terminal human pyrin (amino acids 1–330) expressed and purified by Ni-NTA beads, then incubated in the presence (+) or absence (-) of recombinant PKN1 or PKN2, analyzed by staining with a phosphoprotein gel stain (Pro-Q Diamond) or immunoblot analysis with antibody specific for phosphorylated serine followed by Coomassie blue staining and immunoblot analysis with antibody to Myc (loading control). Data are representative of at least three independent experiments.

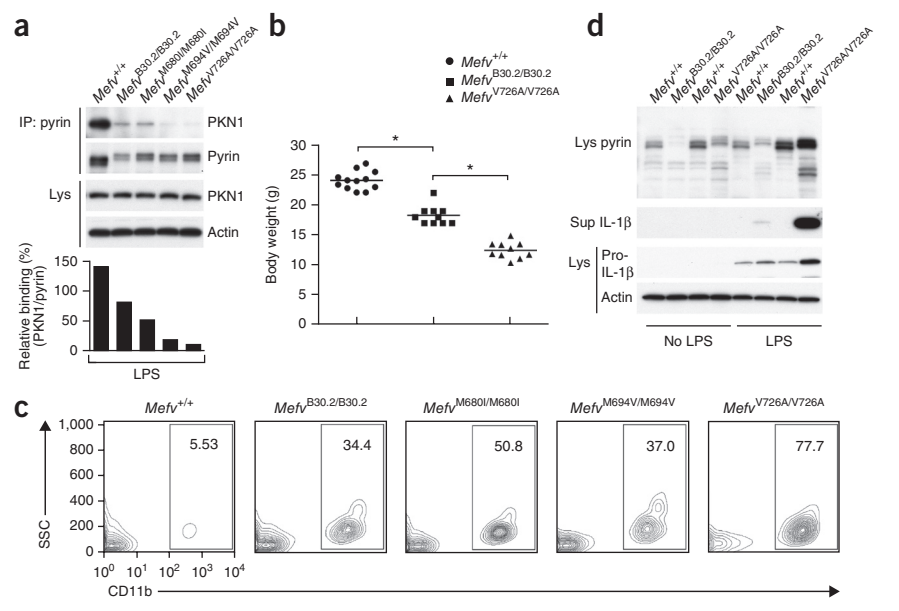


induced spontaneous IL-1 β release, which was dependent on the pyrin inflammasome, and this effect was accentuated when both *Pkn1* and *Pkn2* were knocked down (Fig. 3b,c). However, knockdown of *Rock1* or *Rock2*, or double knockdown of *Rock1* and *Rock2* did not induce IL-1 β release (Fig. 3b), indicating that ROCK1 and ROCK2 are dispensable for regulating the pyrin inflammasome.

Furthermore, we also observed that the pyrin inflammasome was activated in LPS-primed BMDMs by PKC412, a potent inhibitor of PKNs²⁸ (Fig. 4a). Conversely, IL-1 β release from BMDMs treated with C3 toxin or from BMDMs of *Mefv*^{V726A/V726A} mice was markedly inhibited by bryostatin 1, a potent PKC activator (Fig. 4b and

Supplementary Fig. 3b). In contrast, NLRP3 inflammasome activation induced by ATP, AIM2 inflammasome activation induced by double-stranded DNA and NLRC4 inflammasome activation induced by flagellin were not suppressed by bryostatin 1 (Supplementary Fig. 3c). The activation of the pyrin inflammasome was also suppressed by arachidonic acid, a known activator of both PKNs and ROCKs^{29,30} (Fig. 4c and Supplementary Fig. 3d). The effects of arachidonic acid are not as inflammasome-selective as those of bryostatin 1, as arachidonic acid suppressed ATP-driven NLRP3 inflammasome activation through its effects on cAMP^{22,31,32}, although it did not suppress the IL-1 β release induced by NLRC4 or AIM2 inflammasome

Figure 6 The binding of PKN1 to the pyrin of FMF knock-in mice is substantially less than its binding to wild-type mouse pyrin, which lacks a B30.2 orthologous domain, and knock-in mice with the wild-type B30.2 domain of human pyrin have a milder inflammatory phenotype than that of knock-in mice with FMF-associated mutations. (a) Immunoblot analysis of PKN1 and pyrin in LPS-treated BMDMs from wild-type and FMF knock-in (FMF-KI) with wild-type human B30.2 domain or various FMF-associated mutant human B30.2 domains (above lanes), assessed before (Lys) or after (IP) immunoprecipitation with antibody to pyrin. Below, densitometry analysis of PKN1 bands, normalized to pyrin bands. (b) Body weight of 8-week-old male *Mefv*^{+/+}, *Mefv*^{B30.2/B30.2} and *Mefv*^{V726A/V726A} mice. Each symbol represents an individual mouse; small horizontal lines indicate the mean. **P* < 0.0005 (unpaired two-tailed *t* test). (c) Flow cytometry of peripheral blood cells from 8-week-old male *Mefv*^{+/+}, *Mefv*^{B30.2/B30.2}, *Mefv*^{M680I/M680I}, *Mefv*^{M694V/M694V} and *Mefv*^{V726A/V726A} mice. Numbers in outlined areas indicate percent CD11b⁺ myeloid cells. (d) Immunoblot analysis of culture supernatants and lysates of bone marrow CD11b⁺ cells obtained from 8-week-old male *Mefv*^{+/+}, *Mefv*^{B30.2/B30.2} and *Mefv*^{V726A/V726A} mice and treated for 6 h with or without LPS. Data are representative of at least three independent experiments (a,d), one experiment (b) or one experiment with five mice (wild-type and *Mefv*^{M680I/M680I}), seven mice (*Mefv*^{V726A/V726A}) or eight mice (*Mefv*^{B30.2/B30.2} and *Mefv*^{M694V/M694V}) (c).



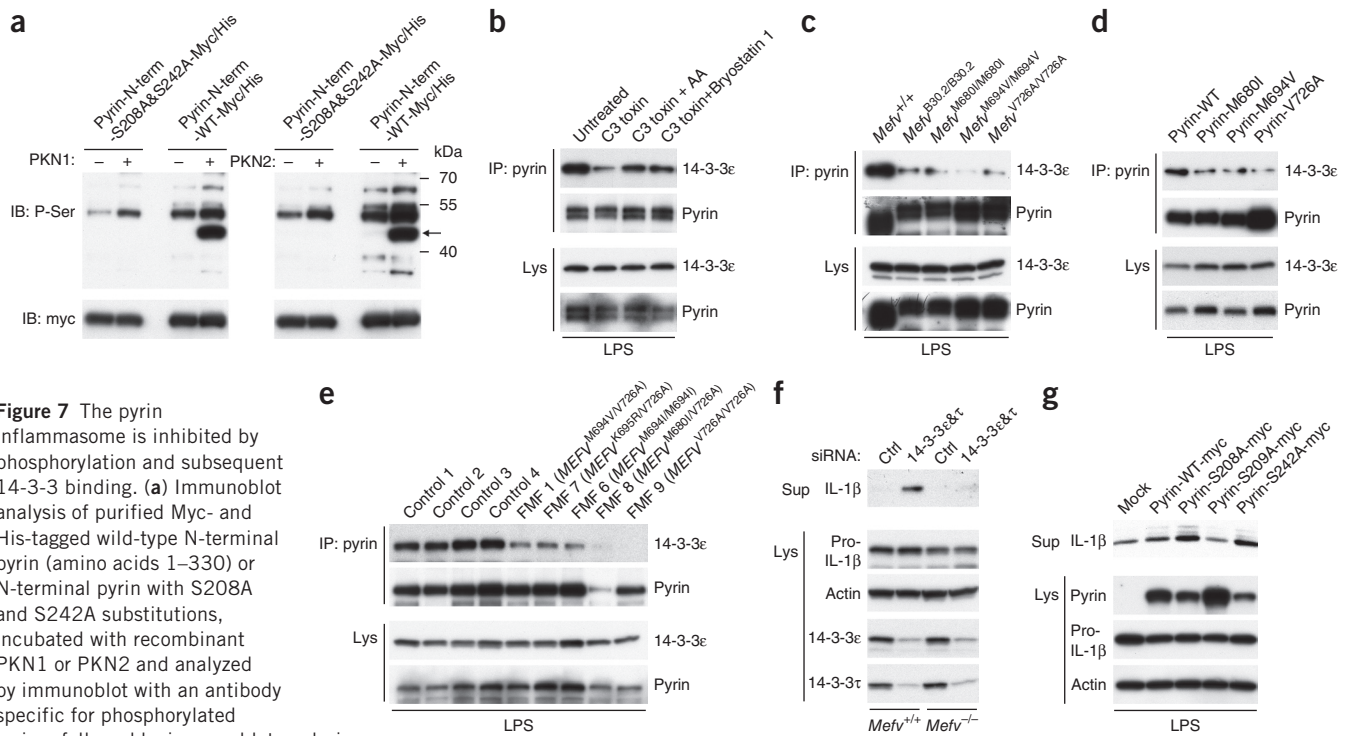


Figure 7 The pyrin inflammasome is inhibited by phosphorylation and subsequent 14-3-3 binding. **(a)** Immunoblot analysis of purified Myc- and His-tagged wild-type N-terminal pyrin (amino acids 1–330) or N-terminal pyrin with S208A and S242A substitutions, incubated with recombinant PKN1 or PKN2 and analyzed by immunoblot with an antibody specific for phosphorylated serine, followed by immunoblot analysis

with antibody to Myc. **(b)** Immunoblot analysis of 14-3-3 ϵ in lysates of wild-type BMDMs treated with LPS, C3 toxin, and either arachidonic acid or bryostatin 1, assessed before and after immunoprecipitation with antibody to mouse pyrin. **(c)** Immunoblot analysis (as in **b**) of LPS-treated wild-type and FMF-KI BMDMs (with wild-type or mutant human B30.2 domain). **(d)** Immunoblot analysis of 14-3-3 ϵ in 239T cells transiently expressing wild-type pyrin or various FMF-associated human mutant pyrin proteins (above lanes), assessed before and after immunoprecipitation with antibody to human pyrin. **(e)** Immunoblot analysis (as in **d**) of macrophages differentiated from PBMCs of four healthy control subjects and five patients with FMF and treated for 16 h with IFN- γ (to induce pyrin expression), then primed for 6 h with LPS. **(f)** Immunoblot analysis of culture supernatants and lysates of wild-type and *Mefv*^{-/-} BMDMs transfected with negative control siRNA or siRNA targeting 14-3-3 ϵ and 14-3-3 τ (14-3-3 ϵ & τ), then treated for 8 h with LPS. **(g)** Immunoblot analysis of culture supernatants and lysates of U937 cells transiently expressing wild-type pyrin or various mutant pyrin proteins (above lanes), primed for 6 h with LPS. Data are representative of at least three independent experiments.

activators (**Supplementary Fig. 3e**). Consistent with the results of the aforementioned siRNA experiments, the constitutive IL-1 β release from PBMCs of patients with FMF was substantially decreased by both PKN activators bryostatin 1 and arachidonic acid (**Fig. 4d,e**). Taken together, these genetic and pharmacological data from murine and human experimental systems support the proposal of a role for PKN enzymes in suppressing the pyrin inflammasome.

PKNs bind to human pyrin and phosphorylate Ser208 and Ser242

To understand how PKNs suppress pyrin inflammasome activation, we tested whether pyrin is a substrate of PKNs. In a co-immunoprecipitation assay, we found an interaction of endogenous pyrin with PKN1 in lysates of LPS-primed BMDMs (**Fig. 5a**). The pyrin-PKN1 interaction was decreased by C3 toxin, but the decreased interaction was restored by co-treatment with arachidonic acid or bryostatin 1 (**Fig. 5a**), indicating that activated PKN1 binds to pyrin and dissociates when PKN1 is inactivated. PKN1 is a serine-threonine protein kinase that has a catalytic kinase domain at its C terminus and an N-terminal regulatory region where activated RhoA and arachidonic acid bind. Human PKN1 interacts with pyrin through this C-terminal kinase domain (**Fig. 5b**), suggesting that pyrin might be phosphorylated. Indeed, direct phosphorylation of pyrin by PKN1 and PKN2 was observed from an incubation of the purified N-terminal half of human pyrin with recombinant PKN1 or PKN2 and subsequent staining of phosphorylated proteins or immunoblot analysis with an antibody to phosphorylated serine (**Fig. 5c**).

We also examined the binding of PKN1 to pyrin in FMF knock-in mice. Most FMF-associated mutations are in sequence encoding the C-terminal B30.2 domain of human pyrin, a domain that is not present in mouse pyrin. We found that the binding of PKN1 to the pyrin of FMF knock-in mice with three frequent FMF-associated B30.2 mutations (*Mefv*^{M680I/M680I}, *Mefv*^{M694V/M694V} and *Mefv*^{V726A/V726A}) was substantially decreased relative the binding of PKN1 to wild-type (*Mefv*^{+/+}) mouse pyrin, which lacks a B30.2 orthologous domain (**Fig. 6a**). The binding of PKN1 to the pyrin of wild-type B30.2 domain knock-in mice (*Mefv*^{B30.2/B30.2}) was also decreased relative to its binding to wild-type mouse pyrin, but was not decreased by as much as it was with the pyrin proteins from *Mefv*^{M694V/M694V} or *Mefv*^{V726A/V726A} mice. *Mefv*^{B30.2/B30.2} mice have been thought to die *in utero*⁵, but we have succeeded in breeding these animals. These mice showed spontaneous inflammatory phenotypes, but the severity as well as IL-1 β release from LPS-primed leukocytes was much lower than that of *Mefv*^{V726A/V726A} mice, which show the most severe inflammation⁵ (**Fig. 6b–d** and **Supplementary Fig. 4a,b**). These findings suggest that the human B30.2 domain has a role in the regulation of PKN1 binding to pyrin.

14-3-3 binds phosphopyrin to inhibit inflammasome activation

Serine residues at positions 208, 209 and 242 of human pyrin have been reported to be phosphorylated and to mediate the interaction with two isoforms of 14-3-3 proteins³³. We found that Ser208 and Ser242 of human pyrin are phosphorylated by PKN1 or PKN2 (**Fig. 7a**)

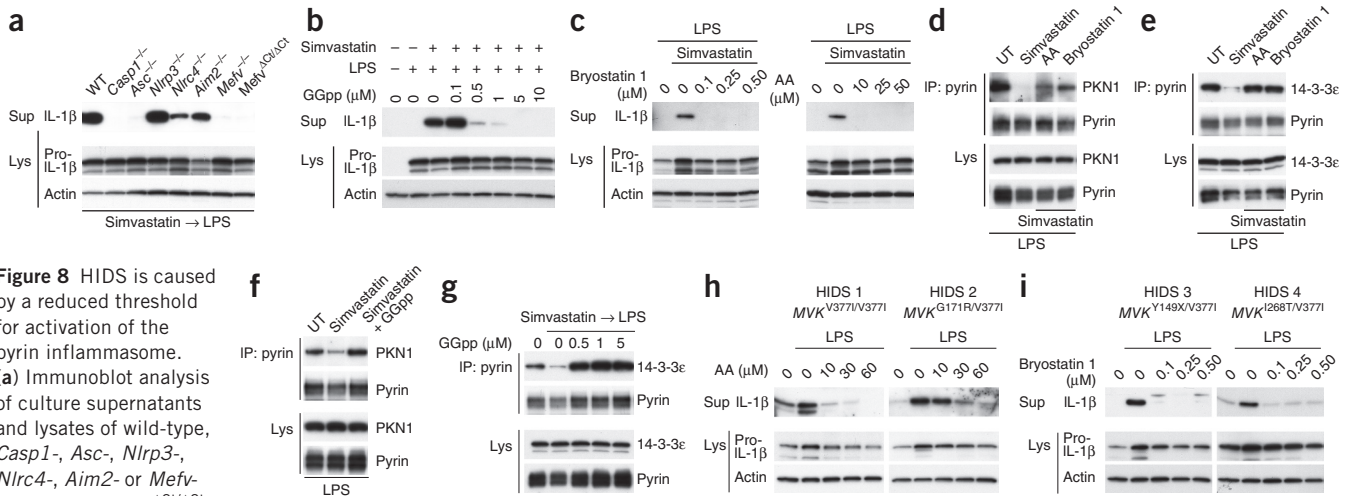


Figure 8 HIDS is caused by a reduced threshold for activation of the pyrin inflammasome. (a) Immunoblot analysis of culture supernatants and lysates of wild-type, *Casp1*^{-/-}, *Asc*^{-/-}, *Nlrp3*^{-/-}, *Nlrp3*^{+/+}, *Nlrp3*^{+/+}, *Nlrp3*^{+/+}, *Nlrp3*^{+/+}, *Mefv*^{ΔCt/ΔCt} BMDMs treated for 16 h with simvastatin (10 μM) and primed for 6 h with LPS. (b) Immunoblot analysis of culture supernatants and lysates of wild-type BMDMs treated for 16 h with simvastatin and then treated for 6 h with LPS plus various doses (above lanes) of geranylgeranyl pyrophosphate (GGpp). (c) Immunoblot analysis of culture supernatants and lysates of wild-type BMDMs treated with LPS, simvastatin (10 μM), and various doses (above lanes) of either bryostatin 1 or arachidonic acid. (d,e) Immunoblot analysis of PKN1 (d) or 14-3-3ε (e) in lysates of wild-type BMDMs treated with LPS, simvastatin, and either arachidonic acid or bryostatin 1, assessed before and after immunoprecipitation with antibody to pyrin. (f,g) Immunoblot analysis of PKN1 (f) or 14-3-3ε (g) in lysates of wild-type BMDMs treated for 16 h with simvastatin and then treated for 6 h with LPS plus GGpp, assessed before and after immunoprecipitation with antibody to pyrin. (h,i) Immunoblot analysis of culture supernatants and lysates of PBMCs obtained from patients with HIDS (1–4) with various mutations in *MVK* (above blots) and treated for 6 h with LPS plus various doses (above lanes) of arachidonic acid (h) or bryostatin 1 (i). Data are representative of at least three independent experiments (a–g) or one experiment (h,i).

and that 14-3-3ε or 14-3-3τ bind to the N-terminal portion of pyrin through Ser208 and Ser242 but not Ser209 (Supplementary Fig. 5a,b). Consistent with the C3-toxin-induced attenuation of the PKN1-pyrin interaction (Fig. 5a), the 14-3-3ε-pyrin interaction was substantially decreased by C3 toxin, an effect that was reversed by PKN activators (Fig. 7b). The binding of 14-3-3ε to mouse pyrin from the FMF knock-in mice was substantially diminished relative to binding to pyrin from wild-type mice (Fig. 7c and Supplementary Fig. 5c), which was also consistent with the PKN1-pyrin interaction (Fig. 6a). In the lysates of BMDMs from *Mefv*^{V726A/V726A} mice, the 14-3-3ε-pyrin interaction was increased by either PKN activation with arachidonic acid or bryostatin 1, or RhoA activation by colchicine (Supplementary Fig. 5d,e). Furthermore, the binding of 14-3-3ε to disease-associated mutant pyrin (M680I, M694V and V726A) was substantially decreased relative to binding to wild-type human pyrin in ectopically expressing 293T cells and macrophages differentiated from the PBMCs of patients with FMF (Fig. 7d,e).

Together with the inhibition of IL-1β release from BMDMs of *Mefv*^{V726A/V726A} mice (Fig. 4b,c) or PBMCs of patients with FMF (Fig. 4d,e) by PKN activation, these findings suggest that the spontaneous activation of the inflammasome in myeloid cells of FMF knock-in mice or patients with FMF might be a result of reduced suppression of pyrin activation by 14-3-3 proteins. Consistent with this hypothesis, spontaneous pyrin-dependent IL-1β release was observed in BMDMs following knockdown of both 14-3-3ε and 14-3-3τ (Fig. 7f). Moreover, ectopic expression of the Ser208A or Ser242A pyrin mutants, which do not interact with 14-3-3, induced IL-1β release in U937 cells without upstream pyrin inflammasome activators, whereas only basal levels of IL-1β were secreted by the non-transfected cells or those expressing wild-type pyrin (Fig. 7g). The binding of 14-3-3 to phosphorylated pyrin therefore acts as a molecular switch to turn off pyrin inflammasome activation that would otherwise occur when either 14-3-3 expression or pyrin serine phosphorylation

is blocked by bacterial toxins, FMF-associated B30.2 mutations or pharmacologic agents (Supplementary Figs. 6 and 7).

The pyrin inflammasome mediates IL-1β release in HIDS

In addition to the GEF-mediated exchange of GDP with GTP on RhoA, the translocation of RhoA from the cytosol to the plasma membrane is essential for its biological function. Membrane targeting of RhoA is dependent on geranylgeranylation at its C terminus. Geranylgeranyl pyrophosphate, the substrate of geranylgeranylation, is a product of the mevalonate pathway. HIDS is caused by loss-of-function mutations in the gene encoding *MVK*. The deficiency in *MVK* function observed in HIDS, or the pharmacological inhibition of 3-hydroxy-3-methylglutaryl-CoA (HMG-CoA) reductase, results in the depletion of geranylgeranyl pyrophosphate, which has been reported to induce IL-1β release in myeloid cells through an unknown inflammasome^{34–36}. Given that RhoA is inactive without geranylgeranylation and that the inactivation of RhoA induces pyrin inflammasome activation, we investigated the role of pyrin in the pathogenesis of HIDS.

Simvastatin, a direct inhibitor of HMG-CoA reductase, induced translocation of RhoA from the membrane to the cytosol and a dose-dependent release of IL-1β from LPS-primed BMDMs (Supplementary Fig. 8a,b). The IL-1β release induced by various HMG-CoA reductase inhibitors—simvastatin, fluvastatin and lovastatin—was dependent on the pyrin inflammasome, but was independent of the NLRP3, NLRP4 or AIM2 inflammasomes (Fig. 8a and Supplementary Fig. 8b–d). We also found that the IL-1β release induced by simvastatin was blocked by supplementation with geranylgeranyl pyrophosphate or activation of PKNs with arachidonic acid or bryostatin 1, which suppress the pyrin inflammasome (Fig. 8b,c and Supplementary Fig. 8e–g).

As seen in cells treated with C3 toxin, simvastatin also substantially decreased the 14-3-3ε-pyrin interaction, as well as the PKN1-pyrin interaction in LPS-primed BMDMs, and these decreased interactions were reversed by the activation of PKNs or by supplementation with

exogenous geranylgeranyl pyrophosphate (Fig. 8d–g). These data indicate that a blockade of the mevalonate pathway induces pyrin inflammasome activation. Of note, the HMG-CoA reductase inhibitor concentrations required to achieve such a blockade were much higher than the blood levels achieved in patients treated with these agents for hypercholesterolemia.

Consistent with the data above, the constitutive IL-1 β release from PBMCs of patients with HIDS was substantially blocked by the suppression of the pyrin inflammasome with arachidonic acid or bryostatin 1 (Fig. 8h,i). Unlike the results obtained for FMF, however, we found little or no inhibitory effect of colchicine on pyrin inflammasome activation in PBMCs of patients with HIDS (Supplementary Fig. 8h), most probably because colchicine could not activate RhoA that was not localized to the cell membrane through geranylgeranylation. These findings indicate an essential role for the pyrin inflammasome in the pathogenesis of HIDS and also provide an ‘experiment of nature’ demonstrating the activation of the pyrin inflammasome by inhibiting the RhoA signaling pathway (Supplementary Fig. 6).

DISCUSSION

By studying RhoA signal transduction, we determined how bacterial toxins activate the pyrin inflammasome. Our central finding, that the pyrin inflammasome is regulated by RhoA-dependent phosphorylation of pyrin and pyrin’s subsequent interaction with 14-3-3 proteins, also delineates the molecular pathogenesis of FMF and defines a previously unknown connection between FMF and the seemingly unrelated autoinflammatory disease HIDS. Our data are consistent with the emerging concept that FMF mutations are gain-of-function with a gene-dosage effect⁵, and the existence of rare FMF mutations at both phosphorylated serine residues of pyrin provides direct evidence of a role for the 14-3-3 proteins in FMF (<http://fmf.igh.cnrs.fr/ISSAID/infervers/>). This concept is strengthened by the description of a previously unknown, dominantly inherited disorder known as ‘pyrin-associated autoinflammation and neutrophilic dermatosis’, which is caused by the pSer242Arg mutation in pyrin³⁷.

Most of the more common and severe FMF-associated mutations are clustered in the C-terminal B30.2 domain of human pyrin. Perhaps as a result of intramolecular interactions, B30.2 domain mutations are likely to control pyrin phosphorylation by inhibiting the binding of kinases to pyrin. Thus, we hypothesize that FMF-associated mutations in the B30.2 domain block the phosphorylation sites from kinases, such as PKN1, resulting in a lowered threshold for activation of the pyrin inflammasome. In mice, which lack a pyrin B30.2 domain, one would expect that the balance would favor the phosphorylated, inhibited state, unless the mouse has evolved phosphatases that tip the balance toward the dephosphorylated, activated state.

Given the extraordinarily high carrier frequency of FMF-associated MEFV mutations in Mediterranean and Middle Eastern populations, the possibility that heterozygous FMF mutations might confer a selective advantage against one or more pathogenic microbes has long been a topic of intense interest. Our findings provide a molecular account of how this may have happened: bacterial toxins that inactivate RhoA have been evolutionarily selected in bacteria because they disable host cell cytoskeletal organization and the numerous downstream host-defense mechanisms, such as leukocyte migration and phagocytosis, that depend on an intact cytoskeleton. The pyrin inflammasome is probably a host counter-measure that resembles the plant guard-type mechanism, allowing hosts to defend against a wide range of pathogens by sensing particular virulence-related activities rather than by sensing pathogen-associated molecular patterns directly^{17,38}.

This hypothesis proposes that the pyrin inflammasome can control a broad spectrum of potential pathogenic infections, perhaps broader than currently appreciated. Normal pyrin exerts its role by nucleating an inflammasome to defend against bacteria, such as *Clostridium difficile*, *Burkholderia cenocepacia* and *Vibrio cholerae*, which utilize toxins to inactivate Rho GTPase, thereby inducing actin depolymerization. The adenylate cyclase toxins secreted from *Bordetella pertussis*, *Bacillus anthracis*, *Pseudomonas aeruginosa* and *Yersinia pestis* induce intracellular accumulation of cAMP in the host cell³⁹. Although the increase of cAMP suppresses the NLRP3 inflammasome²², it conversely potentiates pyrin inflammasome activation. Thus, pyrin may function as an innate immune ‘guard’ in much the same way that R proteins function in plant antimicrobial defense. The requirement for both a priming step and RhoA inactivation prevents pyrin inflammasome activation from being triggered by normal cellular processes. However, the end result is a potent mechanism that defends against a major class of pathogens, and the double-edged sword that is genetic variation in this system of defense.

METHODS

Methods and any associated references are available in the [online version of the paper](#).

Note: Any Supplementary Information and Source Data files are available in the online version of the paper.

ACKNOWLEDGMENTS

We thank the patients enrolled in our clinical protocols for providing research specimens, B. Barham, A. Jones, T. Romeo, P. Hoffmann, D. Stone, P. Pinto-Patarroyo, A. Ombrello and K. Barron for help with caring for patients, I. Aksentijevich for assistance in genotyping patients and for discussions, V. Dixit (Genentech) for ASC-, NLRP3- and NLR4-deficient mice, R. Flavell (Yale University) for caspase-1-deficient mice, E. Alnemri (Thomas Jefferson University) for AIM2-deficient mice, and S. Masters and F. Shao for sharing data before publication. This work was supported by the Intramural Research Program of the National Human Genome Research Institute.

AUTHOR CONTRIBUTIONS

Y.H.P., D.L.K. and J.J.C. designed the study. Y.H.P., G.W. and J.J.C. performed experiments. Y.H.P., G.W., D.L.K. and J.J.C. analyzed the data. Y.H.P., D.L.K. and J.J.C. wrote the manuscript.

COMPETING FINANCIAL INTERESTS

The authors declare no competing financial interests.

Reprints and permissions information is available online at <http://www.nature.com/reprints/index.html>.

- Kastner, D.L., Aksentijevich, I. & Goldbach-Mansky, R. Autoinflammatory disease reloaded: a clinical perspective. *Cell* **140**, 784–790 (2010).
- Masters, S.L., Simon, A., Aksentijevich, I. & Kastner, D.L. Horror autoinflammaticus: the molecular pathophysiology of autoinflammatory disease. *Annu. Rev. Immunol.* **27**, 621–668 (2009).
- The International FMF Consortium. Ancient missense mutations in a new member of the RoRet gene family are likely to cause familial Mediterranean fever. *Cell* **90**, 797–807 (1997).
- Drenth, J.P. *et al.* Mutations in the gene encoding mevalonate kinase cause hyper-IgD and periodic fever syndrome. *Nat. Genet.* **22**, 178–181 (1999).
- Chae, J.J. *et al.* Gain-of-function Pyrin mutations induce NLRP3 protein-independent interleukin-1 β activation and severe autoinflammation in mice. *Immunity* **34**, 755–768 (2011).
- Xu, H. *et al.* Innate immune sensing of bacterial modifications of Rho GTPases by the Pyrin inflammasome. *Nature* **513**, 237–241 (2014).
- Miziorko, H.M. Enzymes of the mevalonate pathway of isoprenoid biosynthesis. *Arch. Biochem. Biophys.* **505**, 131–143 (2011).
- Sohar, E., Gafni, J., Pras, M. & Heller, H. Familial Mediterranean fever. A survey of 470 cases and review of the literature. *Am. J. Med.* **43**, 227–253 (1967).
- French FMF Consortium. A candidate gene for familial Mediterranean fever. *Nat. Genet.* **17**, 25–31 (1997).
- Lachmann, H.J. *et al.* Clinical and subclinical inflammation in patients with familial Mediterranean fever and in heterozygous carriers of MEFV mutations. *Rheumatology* **45**, 746–750 (2006).

11. Booty, M.G. *et al.* Familial Mediterranean fever with a single MEFV mutation: where is the second hit? *Arthritis Rheum.* **60**, 1851–1861 (2009).
12. Marek-Yagel, D. *et al.* Clinical disease among patients heterozygous for familial Mediterranean fever. *Arthritis Rheum.* **60**, 1862–1866 (2009).
13. Ozen, S. Changing concepts in familial Mediterranean fever: is it possible to have an autosomal-recessive disease with only one mutation? *Arthritis Rheum.* **60**, 1575–1577 (2009).
14. Booth, D.R. *et al.* The genetic basis of autosomal dominant familial Mediterranean fever. *Q. J. Med.* **93**, 217–221 (2000).
15. Aldea, A. *et al.* A severe autosomal-dominant periodic inflammatory disorder with renal AA amyloidosis and colchicine resistance associated to the MEFV H478Y variant in a Spanish kindred: an unusual familial Mediterranean fever phenotype or another MEFV-associated periodic inflammatory disorder? *Am. J. Med. Genet.* **124A**, 67–73 (2004).
16. Jones, J.D. & Dangl, J.L. The plant immune system. *Nature* **444**, 323–329 (2006).
17. Mackey, D., Holt, B.F. III, Wiig, A. & Dangl, J.L. RIN4 interacts with *Pseudomonas syringae* type III effector molecules and is required for RPM1-mediated resistance in *Arabidopsis*. *Cell* **108**, 743–754 (2002).
18. Chae, J.J. *et al.* Targeted disruption of pyrin, the FMF protein, causes heightened sensitivity to endotoxin and a defect in macrophage apoptosis. *Mol. Cell* **11**, 591–604 (2003).
19. Schoenwaelder, S.M. & Burridge, K. Evidence for a calpeptin-sensitive protein-tyrosine phosphatase upstream of the small GTPase Rho: a novel role for the calpain inhibitor calpeptin in the inhibition of protein-tyrosine phosphatases. *J. Biol. Chem.* **274**, 14359–14367 (1999).
20. Schmidt, G. *et al.* Gln 63 of Rho is deamidated by *Escherichia coli* cytotoxic necrotizing factor-1. *Nature* **387**, 725–729 (1997).
21. Flatau, G. *et al.* Toxin-induced activation of the G protein p21 Rho by deamidation of glutamine. *Nature* **387**, 729–733 (1997).
22. Lee, G.S. *et al.* The calcium-sensing receptor regulates the NLRP3 inflammasome through Ca²⁺ and cAMP. *Nature* **492**, 123–127 (2012).
23. Lang, P. *et al.* Protein kinase A phosphorylation of RhoA mediates the morphological and functional effects of cyclic AMP in cytotoxic lymphocytes. *EMBO J.* **15**, 510–519 (1996).
24. Aburima, A. *et al.* cAMP signaling regulates platelet myosin light chain (MLC) phosphorylation and shape change through targeting the RhoA-Rho kinase-MLC phosphatase signaling pathway. *Blood* **122**, 3533–3545 (2013).
25. Krendel, M., Zenke, F.T. & Bokoch, G.M. Nucleotide exchange factor GEF-H1 mediates cross-talk between microtubules and the actin cytoskeleton. *Nat. Cell Biol.* **4**, 294–301 (2002).
26. Misawa, T. *et al.* Microtubule-driven spatial arrangement of mitochondria promotes activation of the NLRP3 inflammasome. *Nat. Immunol.* **14**, 454–460 (2013).
27. Allam, R. *et al.* Mitochondrial apoptosis is dispensable for NLRP3 inflammasome activation but non-apoptotic caspase-8 is required for inflammasome priming. *EMBO Rep.* **15**, 982–990 (2014).
28. Falk, M.D. *et al.* Enzyme kinetics and distinct modulation of the protein kinase N Family of kinases by lipid activators and small molecule inhibitors. *Biosci. Rep.* **34**, e00097 (2014).
29. Feng, J. *et al.* Rho-associated kinase of chicken gizzard smooth muscle. *J. Biol. Chem.* **274**, 3744–3752 (1999).
30. Yoshinaga, C., Mukai, H., Toshimori, M., Miyamoto, M. & Ono, Y. Mutational analysis of the regulatory mechanism of PKN: the regulatory region of PKN contains an arachidonic acid-sensitive autoinhibitory domain. *J. Biochem.* **126**, 475–484 (1999).
31. Regan, J.W. EP2 and EP4 prostanoid receptor signaling. *Life Sci.* **74**, 143–153 (2003).
32. Sokolowska, M. *et al.* Prostaglandin E2 inhibits NLRP3 inflammasome activation through EP4 receptor and intracellular cyclic AMP in human macrophages. *J. Immunol.* **194**, 5472–5487 (2015).
33. Jéru, I. *et al.* Interaction of pyrin with 14.3.3 in an isoform-specific and phosphorylation-dependent manner regulates its translocation to the nucleus. *Arthritis Rheum.* **52**, 1848–1857 (2005).
34. Mandey, S.H., Kuijk, L.M., Frenkel, J. & Waterham, H.R. A role for geranylgeranylation in interleukin-1beta secretion. *Arthritis Rheum.* **54**, 3690–3695 (2006).
35. Kuijk, L.M. *et al.* HMG-CoA reductase inhibition induces IL-1beta release through Rac1/PI3K/PKB-dependent caspase-1 activation. *Blood* **112**, 3563–3573 (2008).
36. Normand, S. *et al.* Specific increase in caspase-1 activity and secretion of IL-1 family cytokines: a putative link between mevalonate kinase deficiency and inflammation. *Eur. Cytokine Netw.* **20**, 101–107 (2009).
37. Masters, S.L. *et al.* Familial autoinflammation with neutrophilic dermatosis reveals a regulatory mechanism of pyrin activation. *Sci. Transl. Med.* **8**, 332ra45 (2016).
38. Vance, R.E. Immunology taught by bacteria. *J. Clin. Immunol.* **30**, 507–511 (2010).
39. Ahuja, N., Kumar, P. & Bhatnagar, R. The adenylate cyclase toxins. *Crit. Rev. Microbiol.* **30**, 187–196 (2004).

ONLINE METHODS

Reagents. Ultra-pure flagellin (catalog no. tlr1-pstfla), and ultra-pure LPS (tlr1-pepls) were obtained from InvivoGen. C3 toxin (CT03) and CNF toxin (CN03) were from Cytoskeleton. TcdB toxin (6246-GT) was from R&D Systems. NKH477 (1603), simvastatin (1965), fluvastatin (3309), lovastatin (1530), calpeptin (0448), colchicine (1364), arachidonic acid (2756), bryostatatin1 (2383), staurosporine (1285), and PKC412 (2992) were from Tocris Bioscience. Geranylgeranyl pyrophosphate ammonium salt (G6025) was from Sigma.

Mice. We used 8- to 16-week-old male and female mice (*Mus musculus*) on C57BL/6J background in our experiments. C57BL/6J mice from The Jackson Laboratory were used for WT control. FMF knock-in (KI) mice harboring an FMF-associated mutant human B30.2 domain (*Mefv*^{M680I/M680I}, *Mefv*^{M694V/M694V}, and *Mefv*^{V726A/V726A}), *Mefv*-deficient (*Mefv*^{-/-}), and C-terminal pyrin-truncation mice (*Mefv*^{ΔCt/ΔCt}) have been described previously^{5,18}. Wild-type B30.2 domain KI mice (*Mefv*^{B30.2/B30.2}) were generated by homologous recombination of a targeting construct that has been described in our previous study⁵. Heterozygotes generated from chimeras were crossed with EIIa-Cre transgenic mice (Jackson Laboratory) to remove the neo cassette and backcrossed with C57BL/6J mice at least six generations. ASC-, NLRP3-, and NLRP4-KO mice were a gift from V.M. Dixit (Genentech Inc.). Casp-1-KO mice were from R. Flavell (Yale University). AIM2-KO mice were from E. Alnemri (Thomas Jefferson University). In each experiment, experimental and control mice were age and sex-matched. Both male and female mice were used according to availability. The investigators were blinded to allocation during experiments and outcome assessment for experiments shown in **Figure 6b,c** and **Supplementary Figure 4a,b**. All animal studies were performed according to US National Institutes of Health guidelines and were approved by the Institutional Animal Care and Use Committee of National Human Genome Research Institute.

Patients. Blood specimens from four healthy controls (control 1: 47 years old (Y), male (M); control 2: 53Y, female (F); control 3: 59Y, F; and control 4: 26Y, M), four CAPS (CAPS 1: 17Y, F; CAPS 2: 40Y, F; CAPS 3, 6Y, M; and CAPS 4: 46Y, F), four HIDS (HIDS 1: 8Y, F; HIDS 2: 12Y, M; HIDS 3: 18Y, M; and HIDS 4: 9Y, M) and nine FMF (FMF 1: 16Y, M; FMF 2: 46Y, F; FMF 3: 53Y, M; FMF 4: 53Y, M; FMF 5: 34Y, F; FMF 6: 30Y, M; FMF 7: 77Y, F; FMF 8: 29Y, M; and FMF 9: 82Y, M) patients were drawn after obtaining informed consent under a protocol approved by the National Institute of Arthritis and Musculoskeletal and Skin Diseases/National Institute of Diabetes and Digestive and Kidney Diseases Institutional Review Board.

Cell preparation. BMDMs were obtained by differentiating bone marrow progenitors from the tibia and femur of 6–12-week-old male or female mice in Iscove's Modified Dulbecco's Media (IMDM) containing 20 ng/ml of M-CSF (PeproTech), 10% heat-inactivated fetal bovine serum (FBS, Invitrogen), 1 mM sodium pyruvate, 100 U/ml penicillin, and 100 μg/ml streptomycin (Invitrogen) for 7 d. BMDMs were then replated in 12-well plates 1 d before experiments. Human PBMCs were isolated by LSM-Lymphocyte Separation Medium (50494, MP Biomedicals) from freshly drawn peripheral venous blood from healthy controls or patients and also differentiated into macrophages with 800 units/ml of GM-CSF (PeproTech) for 7 d. Macrophages were treated with 20 ng/ml of IFN-γ (PeproTech) for 16 h and then stimulated with LPS (1 μg/ml) for 6 h.

Site-directed mutagenesis. Mutated human pyrin-expressing constructs were generated by site-directed mutagenesis using QuickChange Lightning Kit (210519-5, Agilent Technologies) according to the manufacturer's instructions. Oligonucleotide primers used to introduce mutations for Ser208Ala were 5'-CGCAGAAACGCCGCTCCGCGGGAG-3' and 5'-CTCCCCGCGGAGCGCGCTTCTGCG-3'. For Ser242Ala were 5'-GATGCGACC TAGAGCCCTTGAGGTAC-3' and 5'-GTGACCTCAAGGGCTTAGGT CGCATC-3'.

Inflammasome activation or inhibition. BMDMs (1.0 × 10⁶ cells per well) or PBMCs (3.0 × 10⁶ cells per well) were plated in 12-well plates in RPMI 1640 (Invitrogen) containing 10% FBS and antibiotics and then primed with 1 μg/ml

LPS in Opti-MEM (Invitrogen) for 6 h. For pyrin inflammasome activation, C3 toxin (0.5 μg/ml) or TcdB toxin (0.5 μg/ml) was added to the medium for 6 h. For depletion of cellular mevalonate levels, BMDMs were incubated with RPMI 1640 medium supplemented with simvastatin, fluvastatin, or lovastatin (1 or 10 μM) overnight. Then medium was replaced with Opti-MEM containing LPS (1 μg/ml) and simvastatin, fluvastatin, or lovastatin for 6 h. For AIM2 or NLRP4 inflammasome activation, 1 μg/ml of dsDNA with 2.5 μl/ml of Lipofectamine 2000 (Invitrogen) or 0.5 μg/ml flagellin with 25 μl/ml DOTAP (Roche), respectively, were mixed in Opti-MEM and incubated for 10 min before treatment of the cells. For NLRP3 inflammasome activation, the medium was replaced with RPMI 1640 medium supplemented with ATP (2 mM) and incubated for 30 min. For the inhibition or augmentation of inflammasome activation, LPS-primed BMDMs were treated with arachidonic acid (10–60 μM), NKH477 (10–500 μM), bryostatatin 1 (0.1–0.5 μM), cardiolipin (0.1–0.5 μg/ml), CNF toxin (0.5 μg/ml), calpeptin (10–50 μM), colchicine (0.1–10⁴ ng/ml), staurosporine (0.1–2 μM), or PKC412 (0.1–5 μM). After 0.5–6 h of treatment, supernatants and cell lysates were collected for immunoblot analysis. None of the reagents in these experiments induced cytotoxicity as confirmed by LDH assay (K311-400, BioVision).

Gene knockdown assay. siRNAs targeting *Pkn1*, *Pkn2*, *Rock1*, *Rock2*, *14-3-3ε* (also known as *Ywhae*), *14-3-3τ* (also known as *Ywhaq*) and negative control siRNA were purchased from Invitrogen. The three siRNAs for *Pkn1* knockdown were 5'-AGAUGACAUCACCCGAUUT-3' (s115927), 5'-GAUC CAGACCUAUGCAAUUT-3' (s115925), and 5'-GAGUGGUGGCGUCG AAAAATT-3' (s203299). The three siRNAs for *Pkn2* knockdown were 5'-CGACAUCAGGAUCGAAUAT-3' (s99524), 5'-GCAGAACCGUA UAGCATT-3' (s99525), and 5'-GCAACCUCCUGAAAACGGATT-3' (s99526). The three siRNAs for *Rock1* knockdown were 5'-GUACCGAACGGACC CUUAAT-3' (s73019), 5'-GGUUGGACUACAGUAAAT-3' (s203580), and 5'-GCGAAUGACUUAUAGGATT-3' (s73018). The three siRNAs for *Rock2* knockdown were 5'-GAGAUUACCUACGGAAAATT-3' (s73020), 5'-GCGGAGAUCAGAAUCGAAT-3' (s73021), and 5'-GGAU GACAAAGCGCAUGUAT-3' (s73022). The three siRNAs for *14-3-3ε* knockdown were 5'-GGCAAUGGUUGAAACUGATT-3' (s76177), 5'-AGGU CUUGCUCUACUUUT-3' (s76178), and 5'-GUAAUCUGUUGUG ACAUUT-3' (s76179). The three siRNAs for *14-3-3τ* knockdown were 5'-CAAGGACUACGGGAGAAAT-3' (s76187), 5'-CAACUAAUCCAGAGA GUAAT-3' (s76186), and 5'-GCAUUGAGCAGAAGACCGATT-3' (s120785). For siRNA gene knockdown experiments, 50–250 pmol siRNA were transfected into BMDMs (10⁶ cells per well) by electroporation and replated in 12-well plates. After 36 h, the siRNA-transfected cells were analyzed for inflammasome activation.

Transfection, immunoprecipitation, immunoblot and ELISA. A total of 2–5 μg of expression constructs for WT or mutant pyrin proteins were electroporated into U937 (ATCC-CRL-1593.2) cells (5.0 × 10⁶ cells) using a Neon transfection system (Invitrogen) in Tip 100-μl tips at 1,500 mV/30 ms/pulse. After transfection, U937 cells were differentiated into macrophages with 400 nM PMA for 48 h and then incubated with Opti-MEM containing 1 μg/ml LPS for 6 h, then supernatants and cell lysates were collected and analyzed by immunoblot for IL-1β.

PT67 (631510, Clontech) or 293T (ATCC-CRL-3216) cells (4 × 10⁶ cells) were plated in 100 mm² cell culture dishes one day before transfection. A total of 0.1–10 μg of expression constructs for WT, FMF-associated mutant, or various domain-deleted pyrin proteins were transfected or co-transfected with expression constructs for full-length or various domain-deleted PKN1 proteins with 10–20 μl of Lipofectamine 2000 according to the manufacturer's instructions. After 36 h, the transfected cells were lysed and incubated with antibodies to myc (1:4,000 dilution; sc-40HRP; Santa Cruz Biotechnology), mouse pyrin (1 μg/ml final concentration; rabbit polyclonal antibody against N-terminal 410 amino acids of mouse pyrin; generated by our laboratory¹⁸) or human pyrin (1 μg/ml final concentration; rabbit polyclonal antibody against N-terminal 374 amino acids of human pyrin; generated by our laboratory⁴⁰). Lysates from BMDMs or human macrophages were immunoprecipitated with 1 μg/ml antibody to mouse pyrin or human pyrin followed by protein A plus agarose (Thermo Scientific). After washing with phosphate-buffered saline

(PBS) or PBS containing 0.05–0.1% SDS (for the immunoprecipitation of WT or FMF-associated mutant pyrin proteins), bound proteins were eluted by 2× SDS sample buffer from the beads and analyzed by immunoblot for PKN1 or 14-3-3 proteins. All cell lines were negative for mycoplasma.

Immunoblots were prepared with Novex Tris-Glycine Gel Systems (Invitrogen) and probed overnight at 4 °C with antibodies to human IL-1 β (1:1,000 dilution; AF-201-NA; R&D Systems); mouse IL-1 β (1:1,000 dilution; AF-401-NA; R&D Systems); caspase-1 (1:200 dilution; sc-514; Santa Cruz Biotechnology), 14-3-3 ϵ (1:1,000 dilution; sc-23957; Santa Cruz Biotechnology); 14-3-3 τ (1:1,000 dilution; sc-69720; Santa Cruz Biotechnology); PKN1 (1:1,000 dilution; sc-393344, Santa Cruz Biotechnology); ROCK1 (1:1,000 dilution; sc-365628; Santa Cruz Biotechnology); ROCK2 (1:1,000 dilution; sc-398519; Santa Cruz Biotechnology); actin (1:5,000; sc-1615HRP; Santa Cruz Biotechnology); myc (1:4,000 dilution; sc-40HRP; Santa Cruz Biotechnology); PKN2 (1:1,000 dilution; 2612; Cell Signaling); or V5 (1:5,000 dilution; R96125; Invitrogen).

Secreted IL-1 β was also measured in supernatant using commercially available ELISA kit according to the manufacturer's instructions (MLB00C, R&D Systems).

Flow cytometry. RBC-lysed single-cell suspensions were obtained from peripheral blood and stained with fluorochrome-conjugated CD11b antibodies in PharMingen Stain Buffer (BSA) (BD PharMingen). Cells were analyzed on FACSCaliber flow cytometer (BD Biosciences) and analyzed with FlowJo software (Three Star).

Measurement of active RhoA-GTP and differential localization of RhoA. BMDMs (2.0×10^6 cells per well) were plated in six-well plates and treated with NKH477 (50–500 μ M), CNF toxin (0.5–2 μ g/ml), or C3 toxin (0.5 μ g/ml) and CNF toxin (0.5–2 μ g/ml). Activated RhoA (RhoA-GTP) levels were measured by RhoA G-LISA Activation Assay kit (BK121, cytoskeleton) and normalized to total RhoA levels, which were measured by Total RhoA ELISA kit (BK150, Cytoskeleton). RhoA-GTP levels of BMDMs treated with C3 toxin (0.5 μ g/ml) and colchicine (10^2 – 10^4 ng/ml) were measured by a pull-down assay with Rhotekin-RBD beads using RhoA activation Assay Biochem Kit (BK036, cytoskeleton). Differential localization of RhoA was determined from membrane and cytoplasmic fractions, which were prepared using the

Membrane and Cytoplasmic Extraction Buffer (MEB and CEB), respectively (78840, Thermo Scientific). Briefly, BMDMs (3.0×10^6 cells per well) were plated in six-well plates and treated with simvastatin (10 μ M) overnight. Cells were scraped with cold PBS and centrifuged at 500 *g* for 3 min. The pellets were resuspended with 100 μ l of CEB and incubated on ice for 10 min. After centrifugation at 500 *g* for 5 min, supernatants were collected as cytosolic extractions. The pellets were resuspended by 100 μ l of MEB by vortexing vigorously and incubated on ice. After 10 min, membrane extractions were collected by centrifugation at 3,000 *g* for 5 min. The isolated membrane and cytosolic fractions were analyzed by immunoblot using antibodies to RhoA (1:1,000 dilution; sc-418; Santa Cruz Biotechnology), calcium-sensing receptor (1:1,000 dilution; ab18200; Abcam), and glyceraldehyde 3-phosphate dehydrogenase (1:1,000 dilution; ab9482; Abcam).

In vitro kinase assay. Myc/His-tagged WT or S208A/S242A mutant N-terminal pyrin (amino acids 1–330) was overexpressed into 293T cells, and the N-terminal pyrin proteins were purified using His-SpinTrap (28-4013-53, GE Healthcare). Each purified N-terminal pyrin protein was incubated with 5 μ g of PKN1 (PR7255B) or PKN2 (PR7370A, Thermo Scientific) at 30 °C for 0.5 h in a kinase buffer (50 mM HEPES pH 7.5, 0.01% BRIJ-35, 10 mM MgCl₂, 1 mM EGTA, 500 μ M ATP and 2.5 mM DTT). The reactants were analyzed by immunoblotting with antibody to phospho-Ser (9606, Cell Signaling) or staining with Pro-Q diamond (P33300, Invitrogen). Pro-Q diamond-stained gel was visualized on Molecular Imager FX (Bio-Rad).

Data analysis, statistics and experimental replicates. Statistical analysis was carried out using a nonparametric Mann-Whitney *t* test, and the unpaired two-tailed *t* test using Prism software (GraphPad). A *P* value of ≤ 0.05 was considered statistically significant. The number of reproduced experimental repeats is described in the relevant figure legends. The investigators were not blinded to allocation during experiments and outcome assessment, except as noted above.

40. Chae, J.J. *et al.* The B30.2 domain of pyrin, the familial Mediterranean fever protein, interacts directly with caspase-1 to modulate IL-1 β production. *Proc. Natl. Acad. Sci. USA* **103**, 9982–9987 (2006).